Geological Quarterly, 2022, 66: 24
DOI: http://dx.doi.org/10.7306/gq.1656

The application of archival borehole data to recognizing the primary mineral composition and diagenetic changes in Jurassic sandy rocks of the Polish Basin

Sara WRÓBLEWSKA[1, 2, *]

[1] University of Warsaw, Faculty of Geology, Żwirki i Wigury 93, 02-089 Warszawa, Poland

[2] Polish Geological Institute – National Research Institute, Rakowiecka 4, 00-975 Warszawa, Poland

Wróblewska, S., 2022. The application of archival borehole data to recognizing the primary mineral composition and diagenetic changes in Jurassic sandy rocks of the Polish Basin. Geological Quarterly, 66: 24, doi: 10.7306/gq.1656

Associate Editor: Piotr Krzywiec

With emphasis being placed on the re-examining of mature petroleum basins and reduction of the negative impact of the industry on the environment, the use of archival data in geological exploration is essential. This is especially important in regions where the old, Soviet-type tools were used in the past and which are now using modern, western logging equipment. The application of archival geological, geochemical and geophysical data allows recognition of reservoir formations without the use of modern measurements. For the purpose of this research, Jurassic sandy rocks identified in the archival borehole Z-GN4 were analysed. They appear to be a perfect target for further petroleum and geothermal exploration in the Polish Basin; however, variable mineral composition and diagenetic features can cause difficulties while estimating their reservoir properties. The difference between gamma ray and spontaneous potential shale volume parameter (clay difference) was applied together with gamma ray measurement to determine the impact of primary and diagenetic features on each sandy petrofacies. Based on an integration of detailed petrographic analysis of available core samples from Z-GN4 borehole with archival borehole logs, four different sandy petrofacies were distinguished. Moreover, deep resistivity and sonic logs were used to highlight the carbonate-cemented intervals. This study shows how the application of petrofacies analysis in archival datasets can support the interpretation of uncored intervals and upgrade the level of reservoir characterization.

Key words: petrofacies analysis, Jurassic sandstones, resistivity log, gamma ray log, spontaneous potential log.

INTRODUCTION

As technology advances, the petroleum industry is increasingly focusing on re-examining mature petroleum basins in order to discover new fields and reduce the negative impact of the industry on the environment. Therefore, using archival data as much as possible is essential. This is especially important in countries where many boreholes have been explored using Soviet-type and where modern logging equipment is now commonly used (Harrison, 1995).

Many archival boreholes drilled from 1950 until 1990 were partially or even fully cored. However, even if the core has been subsequently discarded or destroyed, the borehole documentation is very often supplemented with petrographic and palaeontological descriptions, laboratory data of porosity, density, permeability, and the results of XRD geochemical analyses. Sometimes thin section or cuttings samples are available. Last but not least, well logging measurements were performed for most of the boreholes. Thus, this kind of data is still of irreplaceable geological value. Density and sonic logs are especially important, because of their role in the construction of synthetic seismograms and their application in further seismic interpretation. This is why for decades scientists have been struggling to standardize Soviet-type logs to get useful information from the immense quantity of existing data (Wiltgen, 1994; Harrison, 1995; 1997; Szewczyk, 2000; Furgał, 2003; Wróblewska and Kozłowska, 2019; Epov et al., 2020). While today's trend is to minimize the amount of the core taken, modern geophysical methods like X-tended Range Micro Imaging (XRMI) or Elemental Capture Spectroscopy Sonde (ECS) are more commonly used to identify the mineral composition and easily calculate the petrophysical properties. This is why the integration of diagenetic changes with the different modern well log responses is now being studied (Cui et al., 2017; Lai et al., 2018, 2020). However, there is still room for improvement in terms of correlation with archival datasets by using the traditional methods and log recalculations to minimize the cost of exploration and therefore make this process more efficient and less wasteful of resources.

*E-mail: sara.wroblewska@student.uw.edu.pl

Received: January 11, 2022; accepted: July 4, 2022; first published online: October 4, 2022

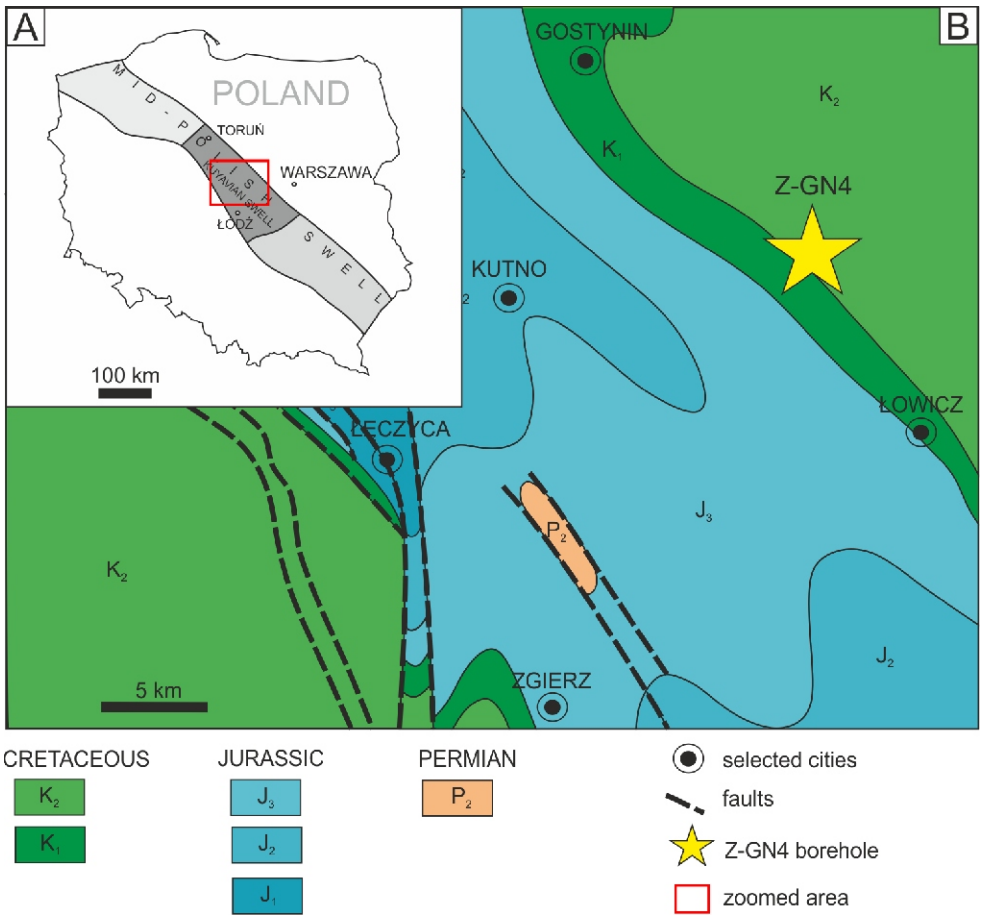

Fig. 1A – location of the research area in Poland (based on Narkiewicz and Dadlez, 2008); B – geological sketch-map (500 m deep) of the Kuyavian segment of the Mid-Polish Swell and the location of the core-section studied (based on Kotański, 1997)

The type of data processing presented in this paper is termed petrofacies analysis and can be used to recognize the probable diagenetic features of reservoir and seal rocks when modern geophysical and geochemical data are missing. Integration of available, archival geological data analysis combined with well log interpretation is still the most accurate and widely used method available, especially for archival datasets, and can be applied by the oil and gas industry to minimize the exploration cost (Ingersoll, 1990; Bhattacharya et al., 2005; De Ros and Goldberg, 2007; Cui et al., 2017; Lai et al., 2018, 2020; Wróblewska and Kozłowska, 2019). This study shows the application of petrofacies analysis to distinguish the best reservoir and seal rock horizons among the not yet fully explored Lower and Middle Jurassic deposits of the Kuyavian segment of the Polish Basin, based on a Z-GN4 core-section.

The Z-GN4 borehole is located within the Kuyavian part of the Mid-Polish Swell (Fig. 1A) which developed as a result of Late Cretaceous–Paleogene regional uplift and inversion of the tectonic unit termed the Mid-Polish Trough (Dadlez et al., 1997; Gutowski et al., 2003; Krzywiec, 2006; Żelaźniewicz et al., 2011). The sandy Jurassic deposits analysed represent a part of the thick, mainly clastic, carbonate, and evaporite infill of the Permian-Mesozoic epicontinental basin. Development of the Mesozoic deposits was governed by regional, thermal subsidence and salt tectonics of the upper Permian (Zechstein) evaporites which began in the Early Triassic (Dadlez et al., 1995, 1998; Marek and Pajchlowa, 1997; Dadlez, 1998; Karnkowski, 1999; Stephenson et al., 2003; Krzywiec et al., 2003; Krzywiec, 2006).

The Jurassic succession of the Kuyavian segment is mainly composed of sandstones, mudstones, shales, and subordinate calcareous sandstones. It has been shown that some of the Jurassic sandstones are characterized by very good reservoir properties, while the mudstones and claystones contain a satisfying amount of mixed oil- and gas-prone kerogen and can be considered as prospective source rocks . However, the variable primary mineral composition of the Jurassic sandstones and therefore its different diagenetic features had a significant impact on the reservoir's parameters as well as on its porosity and/or permeability.

The Lower Jurassic sandy rocks have a continental and shallow marine origin (Pieńkowski, 2004). They are characterized by good reservoir properties; their porosity usually exceeds ~20% and ~1000 mD in permeability. The main factors determining the variation of reservoir parameters in reservoir rocks are compaction, cementation of pore space, and secondary grain dissolution (Krystkiewicz, 1999; Kozłowska and Kuberska, 2014). The Middle Jurassic sandy rocks are represented by the interbedded sandstones, heterolithic deposits and shales with an upwards-increasing carbonate content . They are characterized by moderately good reservoir properties, with porosities usually ~20% and permeabilities varying from 200 to 700 mD (Maliszewska, 1999). Among them, common carbonate-cemented condensed horizons were identified

(Maliszewska, 1998). Similar rocks have been noted in core sections from the North Sea Jurassic successions (Gibbons et al., 1993; Bakke, 1996). Those clastic rocks are composed of detrital material, reworked probably by strong currents associated with a transgressive episode, where the main source of calcite cement was calcareous bioclastic material. Cemented surfaces were also found to be controlled by the depositional bounding surfaces. Because of their characteristic mineral composition, the cemented horizons are clearly detectable on geophysical logs. Moreover, because of their diagenetic features, they may act as a secondary seal for porous, clastic successions.

This study is based on the primary mineral composition of the rocks, their alteration products, and on diagenetic features visible in the thin section. These Jurassic deposits were selected because of their high sandstone content of variable mineral composition which affects the intensity of the natural gamma radiation. Moreover, the presence of kaolinite, as a product of K-feldspar, lithic grains and glauconite alteration can modify porosity and permeability without a significant increase in the gamma ray intensity. The change in petrophysical properties can however be visible on a spontaneous potential curve. The third factor was the presence of carbonate cementation mostly in the upper part of the profile which can have a significant impact on the reservoir properties and can even represent a seal rock. The occurrence of carbonate cements prevents possible fluid flow and usually causes a strong increase in resistivity and decrease in the interval transit time of sonic waves visible on the logs (Bakke, 1996). Even though the cemented layers are only up to a few metres in thickness, their possible lateral extent, associated with depositional bounding surfaces, can have important implications as regards new hydrocarbon discoveries in the Polish Lowland Mesozoic overburden.

GEOLOGICAL SETTING

Lower Jurassic strata in the Polish Basin were deposited in a wide, shallow epicontinental basin surrounded by the Fennoscandian Shield to the north, the Belorussian High and Ukrainian Shield to the east, and the Bohemian Massif to the south-west. Moreover, the land area termed the Pre-Carpathian land was located in the south of the Polish Basin (Dadlez and Marek, 1969; Ziegler, 1990; Deczkowski, 1997; Marek and Pajchlowa, 1997; Dadlez, 1998; Pieńkowski, 2004; Matyja, 2015). Lower Jurassic deposits comprise mainly sandstones, mudstones, and shales with thin, subordinate intercalations of carbonaceous sandstone, lignite, and siderite of continental and/or shallow marine origin, mainly deposited in lacustrine, fluvial, lagoonal, deltaic and/or estuary environments (Feldman-Olszewska, 1997b, 1998; Pieńkowski, 2004). The Middle Jurassic, however, is marked by successively developing transgressions within an extensive epicontinental marine basin (Dayczak-Calikowska, 1964; Dayczak-Calikowska and Moryc, 1988; Feldman-Olszewska, 1997a, 2006) with short regressive episodes in the Early/Late Bajocian and in the Early Callovian (Dayczak-Calikowska and Moryc, 1988; Dayczak- Calikowska, 1997; Kopik, 1998). It comprises mainly marine and subordinate fluvial sandstones and marine, fine-grained deposits, associated with the development of an anoxic shelf. Carbonates, deposited on a shallow marine carbonate ramp and a nodular bed deposited on a starved shelf also formed at the end of the Middle Jurassic.

The main source area of the terrigenous material for Lower and Middle Jurassic sandy rocks of the Polish Basin were probably the Fennoscandian Shield, the Belorussian High and Ukrainian Shield located to the NE. Slow subsidence of the source area, and deepening and the widening of the Middle Jurassic basin in the Callovian and beginning of the Oxfordian, were the reasons why, from the the Early Oxfordian, carbonate sedimention started to gradually dominate over clastic deposition in central Poland. Moreover, the maximum spread of Jurassic deposits across the Polish Basin in the Middle Callovian and Early Oxfordian was the result of relative sea-level rise, probably caused by extensional tectonic movements related to the opening of the Tethys and North Atlantic oceans (Lewandowski et al., 2005; Matyja and Wierzbowski, 2006). The development of carbonate deposition was inhibited by a dissolution process that resulted in nodular, stratigraphically condensed layers and geochemical anomalies in the Middle Callovian. Those rocks are composed of nodular, carbonaceous sandstones and sandy and/or marly limestones with glauconite and/or chamosite and common marine fossils (Premik, 1933; Znosko, 1957, 1968; Feldman-Olszewska, 1997a). These characteristic layers were initially mentioned by Michalski (1885) and informally distinguished as „nodular beds". These deposits dominated carbonate deposition until the Early Oxfordian when the carbonate sedimentation started to accelerate.

The Lower Jurassic sandstones are composed mainly of quartz with a very small amount of feldspars, lithic grains, and/or muscovite (Teofilak, 1960, 1961, 1962; Marek and Pajchlowa, 1997; Krystkiewicz, 1999; Kozłowska and Kuberska, 2014). Clay matrix (if present) comprises illite, kaolinite, quartz, iron hydroxides, and organic matter. Authigenic minerals are represented mainly by kaolinite, quartz overgrowths, and different types of early and late diagenetic carbonates. According to Kozłowska and Kuberska (2014) and Krystkiewicz (1999), diagenesis of Lower Jurassic sandstones in the Kuyavian segment of the Polish Basin took place in three stages. In the first stage of diagenesis, early mechanical compaction and feldspar/muscovite dissolution began (Fig. 2). At the same time the first generation of quartz, kaolinite, and microcrystalline siderite cementation was initiated. During late diagenesis, the next generations of siderite, calcite, ankerite and fibrous illite started to form, while the dissolution of unstable grains still continued. Among the major diagenetic processes affecting the Jurassic sandstones are compaction, cementation, and dissolution. Authigenic quartz cementation is one of the reasons why the primary porosity is still important in the total Lower Jurassic sandstone porosity. Nevertheless, secondary porosity caused by the kaolinization of feldspar grains also increases the total rock porosity which usually exceeds 20% with permeability exceeding 1000 mD (Kozłowska and Kuberska, 2014).

Sandy strata of Middle Jurassic are represented by sandstones and heterolithic deposits. Siderite intercalations and/or concretions were also noted together with highly calcareous sandstones. (Maliszewska, 1999). Quartz is the main component of the grain framework, but lithic grains and feldspars are also common. Moreover, muscovite, biotite, pyrite, glauconite, and heavy minerals are visible in smaller amounts. In the clay matrix, kaolinite and locally chlorite are dominant (Teofilak, 1962; Teofilak-Maliszewska, 1968). An essential role in lithification of the Middle Jurassic sandy rocks was played by diagenetic processes such as compaction, cementation, dissolution, replacement and alteration. In the lower part of the Middle Jurassic succession, siliceous cementation is common and carbonates occur only occasionally. However, in the upper part of the Middle Jurassic deposits of the Bathonian and Callovian, calcareous cement dominates and is represented by Mn-/Fe calcite, siderite, dolomite and ankerite (Teofilak-Maliszewska, 1968; Maliszewska, 1999).

Most of these processes took place during eo- and mesodiagenesis (Fig. 2). Highly mineralized fluids from Zechstein salt are considered as the main source of elements

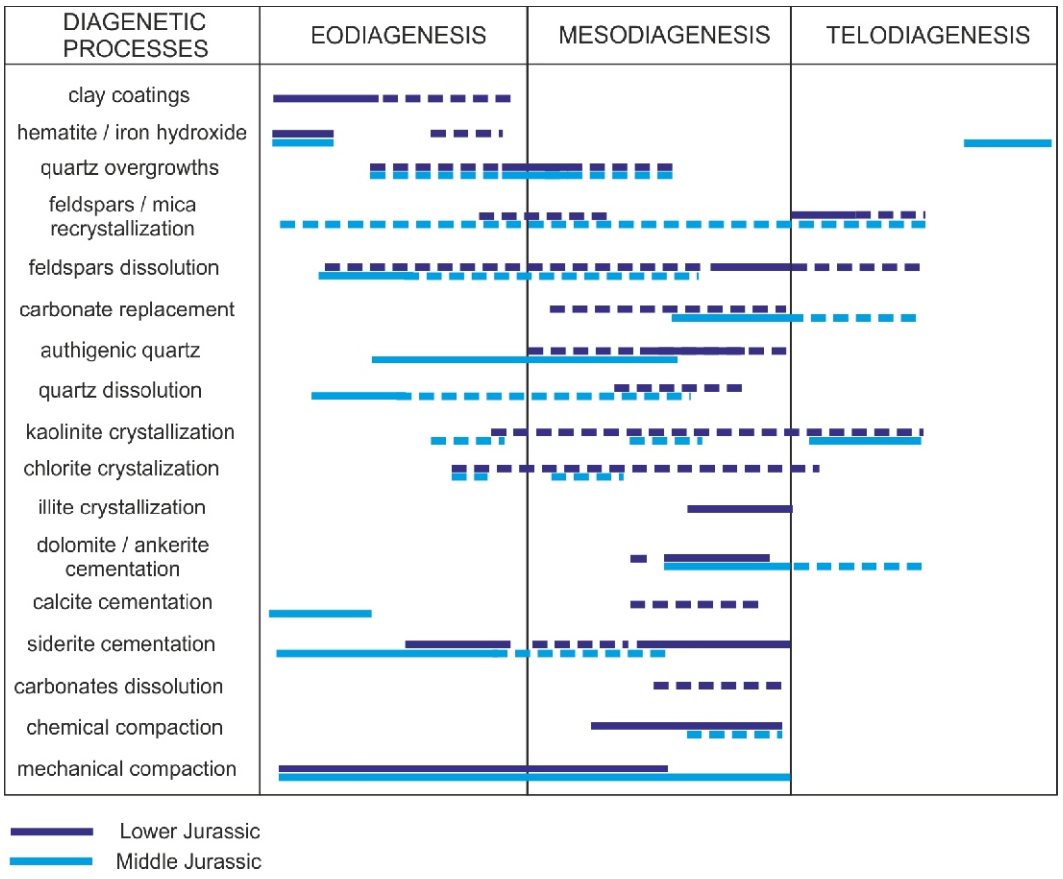

Fig. 2. Diagenetic sequence of the Lower and Middle Jurassic (based on Maliszewska, 1999; Krystkiewicz, 1999; Kozłowska and Kuberska, 2014)

Dotted line – uncertain extent

that influenced the authigenic mineralization and recrystallization processes in the Middle Jurassic sandstones, in particular the carbonates, hematite, and feldspar overgrowths (Znosko, 1957; Teofilak-Maliszewska, 1968). In the early burial stage, the generation of calcite and microcrystalline siderite cement took place. Dissolution and recrystallization of calcareous bioclasts are the main indicators of this generation of calcareous cement. Secondly, primary calcite cementation was replaced by dolomite and/or ankerite. After regional uplift in the Cretaceous/Paleogene, some of the processes, such as the kaolinization of feldspars, were accentuated because of the infiltration of meteoric water (Maliszewska, 1999). Despite the strong influence of diagenetic processes, the Middle Jurassic rocks usually show moderately good reservoir properties – the porosity values of sandstones usually exceed 10% and permeability most frequently rises to 700 mD.

MATERIALS AND METHODS

The results described below were obtained based on lithological description of the core material, petrographic analysis of 11 available archival thin sections, and geophysical data from the Z-GN4 borehole, located in the Kuyavian part of the Mid-Polish Swell (Fig. 1). This core-section was chosen based on the thickness (1152.5 m) of the clastic Jurassic succession and the availability of archival core samples, geophysical well log data, and documentation prepared by Karelus et al. (1992). The borehole documentation includes a basic stratigraphic interpretation (Marek et al., 1992), petrophysical measurements (porosity, density and permeability), and results of geochemical XRD analysis (Kopczyński et al., 1992).

The base of the Lower Jurassic deposits in the Z-GN4 borehole was recognized at a depth of 2822.5 m (Karelus et al., 1992) as a visible transition between reddish Upper Triassic fine-grained deposits and an 81 m-thick sandstone succession. The top of the Middle Jurassic is marked as a carbonate level at a depth of 1670 m.

To properly correlate the well data, macroscopic analysis of the available core samples was carried out. Lithology, grain size of clastic rocks, colour, sedimentary structures, HCl reaction, presence of charred plant detritus, and the visible mineralogical components of the sandy rocks were taken into account. The last of these have a significant influence on petrophysical parameters and/or disrupt the geophysical measurements, such as muscovite, glauconite, kaolinite or potassium feldspars.

Petrographic analysis of available sandstone thin sections (Table 1) focused on primary features such as grain size, primary mineral composition, the type and content of matrix, texture, and diagenetic features such as cements, the character of grain contacts, and mineral alteration products, necessary to define reservoir sandstone parameters. To classify the sandstone, the percentage of quartz, feldspars, and lithic grains were estimated using the grid-point counting method based on 300 points per sample. Each sample was described according to the sandstone classification of Pettijohn et al. (1974). *NIS-Elements* software was used to take microphotographs of the samples.

Table 1

Results of petrographic analysis of sandstone thin section samples from the Z-GN4 core section

Sample	Depth [m]	Q [%]	F [%]	L [%]	Other [%]	Cement / matrix [%]	[%]	Lithology	Diagenetic features
37	1702.2	74	16.5	2	heavy minerals, muscovite (2.5)	hematite (3)	2	heterolith	kaolinization of feldspars, illitization of muscovite, quartz overgrowths
39	1703.25	24	8.5	3	–	carbonate (62)	2.5	calcareous subarcosic arenite / sandy limestone	kaolinization of feldspars, quartz overgrowths
42	1704.65	26.5	18	2.5	–	carbonate (43)	10	arkosic arenite	kaolinization of feldspars, cement dissolution
44	1815.25	39.75	0	2	bioclasts (5)	carbonate (52%)	1.25	clayey-sandy siderite	siderite
57	2119.95	78	0.75	2.5	–	clay matrix (3.25)	15.5	quartz arenite	clay coatings
62	2122.75	80.5	0	2.5	–	–	17	quartz arenite	quartz overgrowths
69	2260.45	60	3.5	11.25	muscovite, heavy minerals (0.25)	–	25	sublith arenite	kaolinization of feldspars
92	2447.45	78	3	1	–	kaolinite pseudomatrix	18	quartz arenite	kaolinite cementation
100	2539.45	66.5	20	1.5	muscovite (4)	carbonate (1)	7	subarkosic arenite	illitization of muscovite and feldspars, kaolinization of feldspars
103	2652.25	72.5	22.5	0.5	muscovite (2)	carbonate (1)	1.5	subarkosic arenite	quartz overgrowths, illitization of muscovite and feldspars, kaolinization of feldspars
104	2652.65	73.25	2.5	5.75	–	carbonate (4)	14.5	sublitharenite	quartz overgrowths, illitization of muscovite, kaolinization of feldspars

Q – quartz, F – feldspars, L – lithic grains, - porosity

The archival geophysical data had to be converted and normalized because of the different accuracies of the Soviet-type tools used in the borehole analysed. The gamma ray intensity, primarily measured in counts per minute (cpm), was converted by the author into standard gamma ray units (API) according to Harrison (1995) and Bolesta and Gałązka (2014) using the lithology benchmark linear recalculation method. A maximum gamma ray value was chosen for shales (200 API), and minimum for quartz sandstones (5 API). This conversion was important to estimate rock parameters and to integrate the gamma ray intensity for further research (Jarzyna et al., 1999; Bolesta and Gałązka, 2014).

Porosity and permeability laboratory data together with archival XRD results were taken from the Z-GN4 borehole documentation prepared by Karelus et al. (1992). Geochemical analysis was performed by X-ray diffraction, with a copper x-ray tube with a graphite crystal monochromator. The tube was characterized by exposure parameters of 40kV of and 25mA. The goniometer shift was 2°29'/min with the paper shift of 2 cm per minute. Reinforcement for powder samples was 1 10^3 cpm.

The results of the petrographic analysis, especially primary and secondary mineral composition, together with textural features, were compared with geophysical parameters of the rocks analysed and archival geochemical and petrophysical results from the borehole documentation (Karelus et al., 1992). Firstly, sandy rocks in uncored intervals of the Lower and Middle Jurassic succession in the Z-GN4 borehole were identified based on cuttings samples and geophysics [low natural gamma radioactivity, spontaneous potential, compressional slowness and laterolog (resistivity) measurements]. Finally, four sandy petrofacies were distinguished. The term petrofacies was used to describe a sandy lithotype with specific petrographic, petrophysical, and geophysical characteristics. Each of these is characterized by the limits of geophysical measurements based on the chemical and physical features of primary and secondary rock components. The diverse primary and secondary mineral composition of the sandstones analysed was the main reason to apply the difference between gamma ray and spontaneous potential shale volume. The method was first applied by the author and termed as the clay difference calculation. Linear shale volume parameter (*Vsh*) in both cases was calculated for the whole profile based on the maximum and minimum measurements taken for quartz arenite and shale which correspond to grain framework (GR_{clean} = 5 API; SP_{clean} = 1 mV) and clay matrix values (GR_{shale} = 200 API; SP_{shale} = 170 mV). Moreover, deep resistivity and sonic logs were used to recognize the strongly carbonate-cemented intervals.

SANDY ROCKS PETROGRAPHY

The sandstones from Z-GN4 borehole represent quartz, subarkosic, arkosic, and sublith arenites (Table 1); quartz is the main component. Most observed rock fragments are of quartzite and sandstone represented by polycrystalline quartz. Alkaline feldspars predominate over plagioclase content. Muscovite grains, heavy minerals, and organic matter are rarely visible as a grain framework components.

In the Z-GN4 thin sections, various types of diagenetic mineralization were observed which can both improve and deteriorate the petrophysical properties, and also modify the geophysical properties of the rock. Most commonly in the Jurassic sandstones, kaolinite derived from the alteration of feldspars, glauconite, and/or lithic grains occur in the pore space (Fig. 3C) or as a replacement of detrital grains, usually feldspars or unstable lithic clasts (Fig. 3B, D). Illitization of feldspars and/or muscovite grains is visible in the deeper part of the profile (Fig. 3B). In the top interval, carbonate cement is common (Fig. 4) in some cases exceeding 50% of the rock. The grain framework in the carbonate-cemented sandstones is usually dispersed, which suggests early carbonate cementation (Fig. 4). Moreover, some of the grain framework components are replaced or corroded by the carbonate mineralization (Fig. 4). Carbonates are represented mostly by dolomite and siderite, as indicated by the archival XRD results from borehole documentation (Kopczyński et al., 1992). Authigenic quartz cements are also visible in some parts of the profile (Fig. 3E). Characteristic rhombohedral dolomite crystals shape can be observed in sample 42 (Fig. 4B) and microcrystalline siderite in sample 44 (Fig. 4D). Hematite mineralization was observed in the uppermost part of the profile analysed which, together with kaolinite, can be a result of glauconite alteration in mixed carbonate and clastic deposits (Fig. 3D).

The porosity of these Jurassic sandstones is usually high, in Z-GN4 locally exceeding 25%. In thin sections, the high porosity is usually secondary and appears as a microporosity between the kaolinite crystals substituting feldspar and/or lithic grains. In places kaolinized grains can even form a pseudomatrix between more resistant quartz grains (Fig. 3C). Preservation of primary porosity was possible in less compacted sandstones, where the clay coatings prevented the quartz cementation of the pore space and in sandstones where quartz overgrowths prevented the primary porosity from compaction. Heterolithic deposits commonly have very low porosity but recognizable borrows can be treated as a possible pethway of migration (Fig. 3A).

INTERPRETATION OF GEOPHYSICAL DATA

THE GAMMA RAY AND SPONTANEOUS POTENTIAL SHALE VOLUME COMPILATION – CLAY DIFFERENCE LOG

Gamma ray and spontaneous potential logs are commonly used in the petroleum industry to calculate the volume of shale in sandy formations (Jahan et al., 2007; Adeoti et al., 2009; Szabó, 2011). However, the mode of action of both measurements varies and can be modified by different factors which can dramatically disrupt the petrophysical calculations. This is especially important when the modern mineralogical logs are missing.

Gamma ray measurement is a record of a formation's radioactivity which is emanated by naturally occurring uranium, thorium, and potassium (Serra, 1986; Rider, 2002). Therefore, it is an excellent estimator of shale volume in quartz arenite formations, where the shale content is associated mainly with primary clay matrix rich in potassium-rich illite. However, many other components can raise gamma ray measurements such as potassium feldspar and muscovite, and thus overstate calculated shale volume. Nevertheless, some clay minerals such as kaolinite, chamosite and chlorite in their typical chemical state emit very little or no radioactivity which usually makes them invisible or only slightly visible on gamma ray logs, thus for the proper estimation of clay content an additional method needs to be applied.

Spontaneous potential is a measurement of the natural difference of self-potentials between an electrode placed in the borehole and on the surface (Serra, 1986; Rider, 2002). The analysis of SP measurements is a perfect method to distinguish permeable intervals in shaly/cemented sandstones, heterolithic deposits and/or shales (Adeoti et al., 2009; Szabó, 2011; Willis et al., 2017). However, to recognize the direction of the SP curve deflection (negative or positive) between permeable and impermeable layers, the relationship between the salinity of formation water (~65 g/l) and mud filtrate must be considered. The salinity of formation water in the interval analysed was higher than the salinity of mud filtrate, and this relationship remained stable. In this type of relation, clay layers show positive values, while sandy layers indicate only negative. The formations analysed were fully saturated with reservoir water.

Combined calculations based on gamma ray and spontaneous potential measurements give important information on the type of primary and/or secondary clay minerals in shaly/sandy rocks rich in K-rich mineral components. For this study, the difference between gamma ray and spontaneous potential shale volume was applied to recognize the primary and secondary mineral composition of the sandstone.

The linear shale volume parameter (*Vsh*) in both cases was calculated for the whole profile based on the maximum and minimum measurements taken for quartz arenite and shale which correspond to grain framework (GR_{clean} = 5 API; SP_{clean}= 1 mV) and clay matrix values (GR_{shale} = 200API; SP_{shale} = 170 mV).

$$Vsh_{GR} \quad \frac{GR_{LOG} \quad GR_{clean}}{GR_{shale} \quad GR_{clean}} \qquad [1]$$

$$Vsh_{SP} \quad \frac{SP_{LOG} \quad SP_{clean}}{SP_{shale} \quad SP_{clean}}$$

where: GR_{LOG} / SP_{LOG} – *GR/SP* log reading; GR_{clean}/SP_{clean} – *GR/SP* log reading measured for clean quartz arenite; GR_{shale}/SP_{shale} – *GR/SP* log reading measured for shale.

There is a difference in shale volume calculated by the *GR* and *SP* logs, and so the new method was applied. The variable which is a subtraction result of Vsh_{SP} and Vsh_{GR} was calculated to make the comparison clearer and easily applicable in recognizing the mineral composition and diagenetic features of the sandstone (Fig. 5 and Table 2).

RESISTIVITY AND SONIC LOG RESPONSE IN CARBONATE-CEMENTED SANDSTONES

The resistivity log shows the response of the formation and its contained fluids to the passage of an electric current (Serra, 1986; Rider, 2002). Therefore, porosity and rock texture, geometry of the pores filled with formation water, or more specifically, the connections of the pore spaces, are the main factors that determine the rock resistivity. Carbonate-cemented layers are characterized by distinctly higher resistivity. In this study, the 15 ohmm value was taken to distinguish highly cemented sandstone layers.

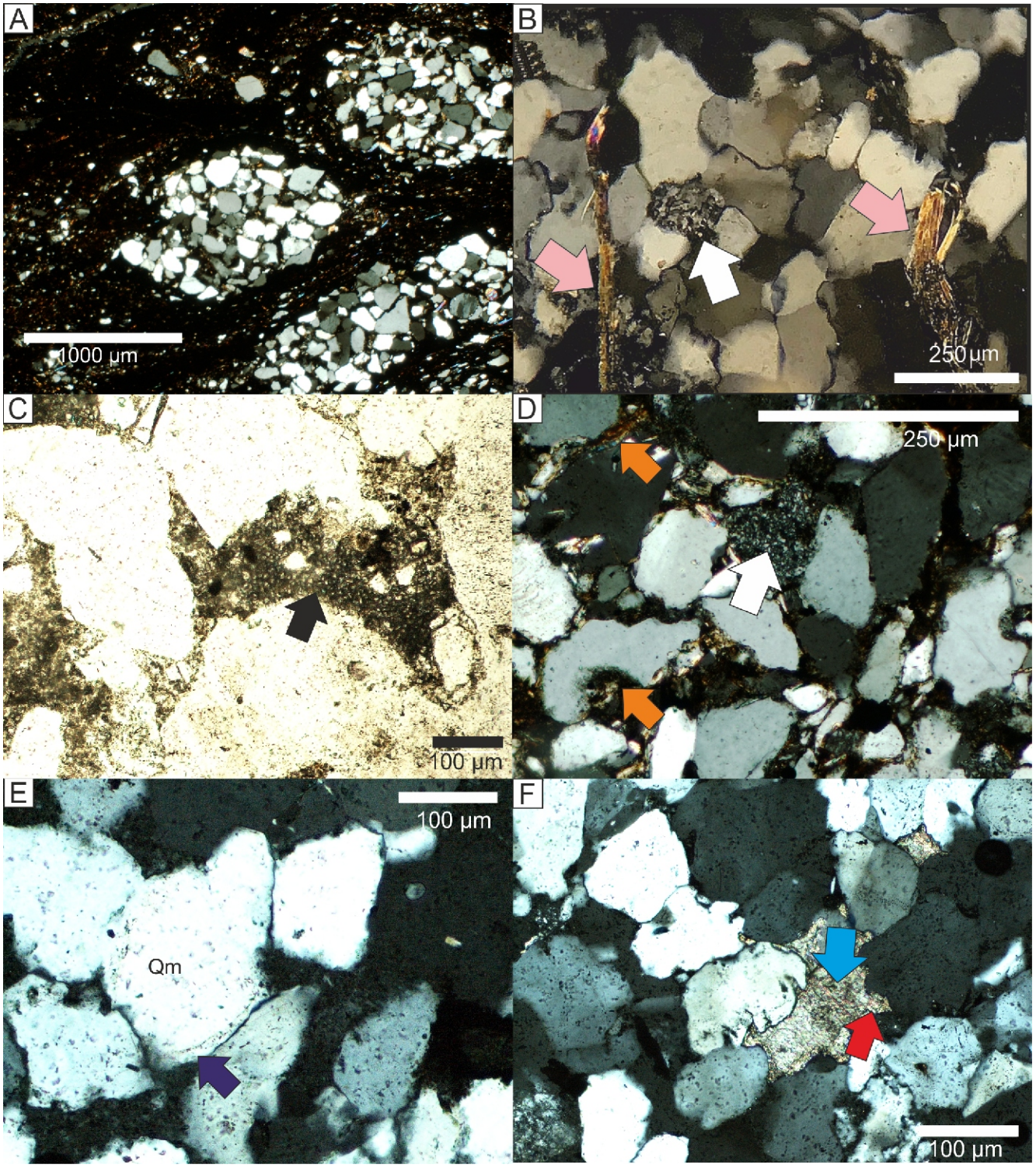

Fig. 3. Microphotographs of sandstones from the Z-GN4 borehole

A – burrows, sample 37, crossed polars, depth: 1702.2 m; **B** – alteration of feldspar and muscovite grains, sample 100, crossed polars, depth: 2539.45 m; **C** – kaolinite derived from the alteration of feldspars, glauconite, and/or lithic grains, sample 92, plane parallel light, depth: 2447.45 m; **D** – hematite mineralization, sample 37, crossed polars, depth: 1702.2 m; **E** – quartz overgrowths, sample 103, crossed polars, depth: 2625.25 m; **F** – grain corrosion by carbonate mineralization, sample 104, crossed polars, depth: 2652.65 m; Qm – monocrystalline quartz, light blue arrow – calcareous cement, black arrow – kaolinite filling of pore-space / clay coating, light pink arrow – illitization of muscovite grains white arrow – kaolinite replacement of detrital grain, orange arrow – hematite mineralization, red arrow – grain corrosion

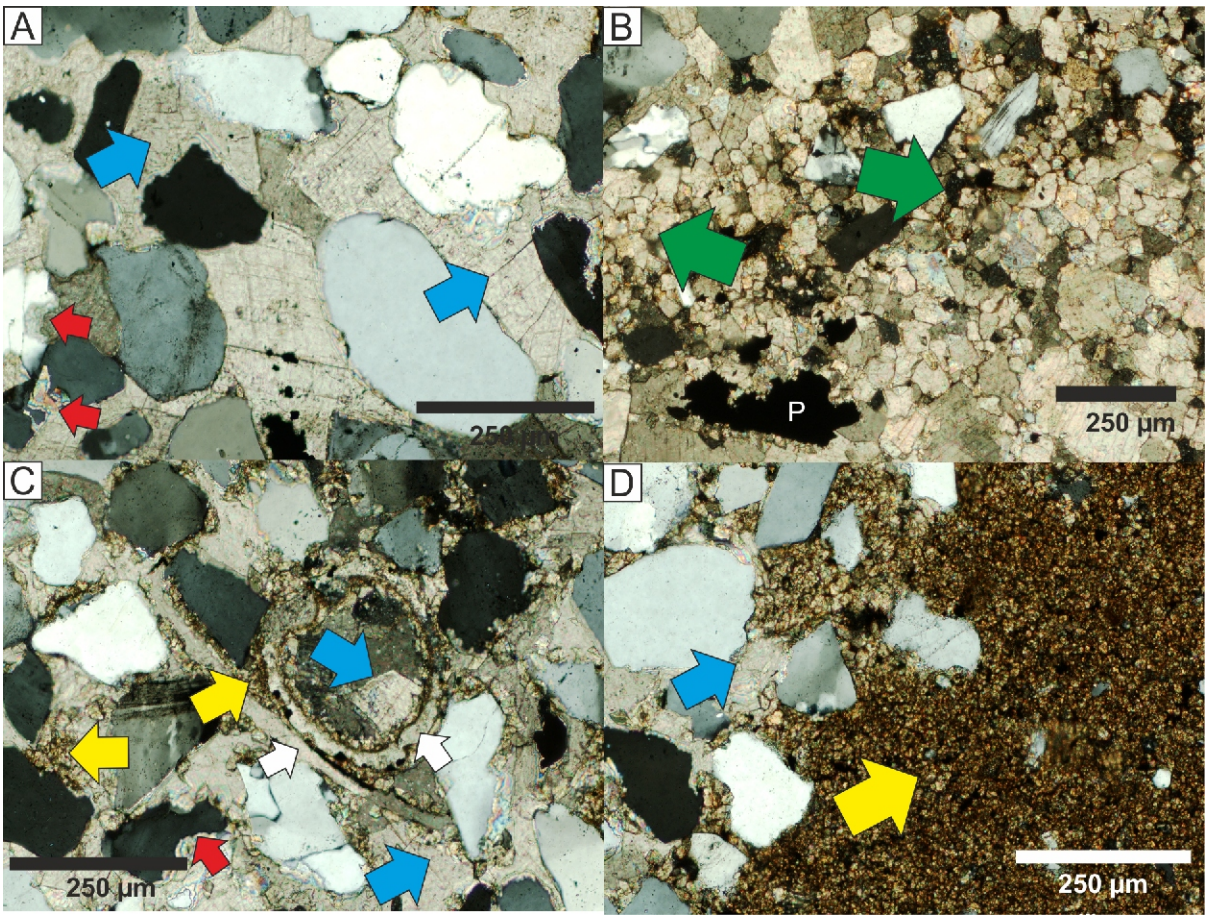

Fig. 4. Microphotographs of calcareous sandstones from the Z-GN4 borehole

A – calcareous cement and grain corrosion in sample 39, crossed polars, depth: 1703.25 m; **B** – calcareous cement and rhombohedral crystals in sample 42, crossed polars, depth: 1704.65 m; **C, D** – microcrystalline siderite, sample 44, crossed polars, depth: 1815.25 m; P – pore space, yellow arrow – microcrystalline siderite, green arrow – dolomite rhombohedral crystals, red arrow – grain corrosion, blue arrow – calcareous cement, white arrow – calcareous echinoderm microfossils

Table 2

Clay difference values compared with probable primary and/or diagenetic influential factors defined by author

GR values	Clay difference values	Possible primary and/or diagenetic influential factors
0–30 API	<(–0.15)	– quartz arenites or quartzitic litharenites, – non-radioactive clay minerals, – intense compaction, – quartz or carbonate cementation
	>(–0.15)	– quartz arenites, – high primary porosity saved by the presence of clay coatings which prevented the development of quartz overgrowths, – the presence of quartz cementation has prevented the compaction process
30–70 API	<(–0.15)	– (sub-) arkosic and/or shaly sandstones, heterolithic deposits and clayey sandy siderites, – muscovite, – intense carbonate cementation, – condensed layers with high uranium content
	>(–0.15)	– subarkosic/sublithic arenites and/or shaly sandstones, – muscovite, – slight carbonate cementation, – illitization, – secondary porosity

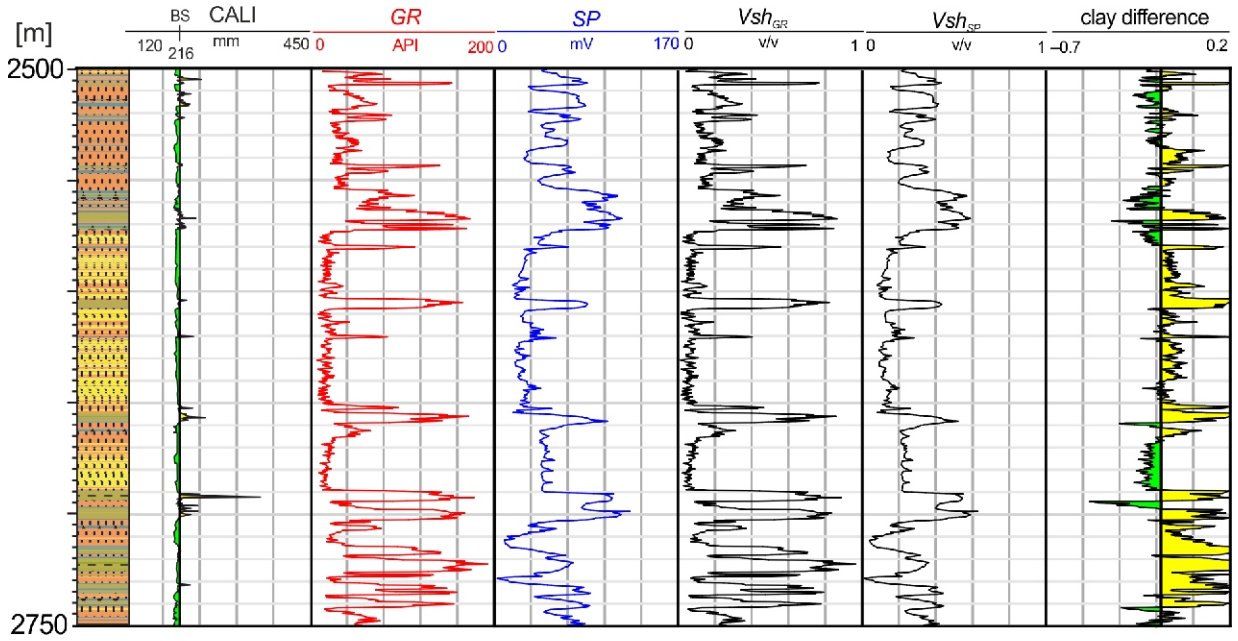

Fig. 5. Model of clay difference log generation from *SP* and *GR* shale volume

The sonic log is a second measurement highly sensitive to subtle textural variations. It shows the formation's capacity to transmit sound waves by the measurement of the interval transit time (*t*) in the formations: the reciprocal of the velocity (Serra, 1986; Rider, 2002). The velocity of the rock is measured as a sum of grain matrix velocity and velocity of the interstitial fluid present in the pore space. Here, a maximum compressional slowness of ~90 μs/ft (246 μs/m) for carbonate-cemented layers was taken for a rock with a grain framework composed of 40% quartz (55.5 μs/ft), 5% K-feldspars (~47 μs/ft), 20% carbonate cement (47 μs/ft), 10% clay (167 μs/ft) content and 25% secondary porosity filled with formation water (200 μs/ft) calculated using the standard Wyllie's equation:

$$t \quad t_f \quad 1 \quad t_{ma} \qquad [2]$$

where:· – total porosity of the rock; t_f – velocity of interstital fluids (ft/sec); t_{ma} – velocity of the rock matrix (ft/sec)

The carbonate-cemented rock samples analysed show lower values of ~60/70 us/ft depending on the mineral composition, clay content and percentage of carbonate cementation.

RESULTS

The integration of petrographic rock features and log responses was the basis to distinguish four different sandy petrofacies. For each petrofacies, representative intensities of natural gamma ray and clay difference were determined (Table 3 and Fig. 6).

Petrofacies have been categorized based firstly on gamma ray values. 30 API was the limit value (boundary on the plot in Figs. 6 and 7) chosen to divide clean quartz/sublithic from sub-/arkosic sandstones and heterolithic deposits based on available core samples and thin sections. Secondly, each petrofacies was analysed for the effects of diagenetic processes visible in thin sections and further compared with the clay difference (positive/negative) values calculated from the

Table 3

Representative ranges of gamma ray intensity and clay difference values for sandy petrofacies

Petrofacies	Petrography of sandy rocks	Influential factors		Type of porosity	Gamma ray intensity [API]	Vsh_{GR}–Vsh_{SP}	Core samples numbers
		radioactive	non-radioactive				
S1	quartz and sublitharenites	–	quartz overgrowths, calcareous cementation, kaolinite	secondary	0–30	<(–0.15)	69, 92
S2		clay coatings	quartz overgrowths	primary		>(–0.15)	57, 62,
S3	subarkosic sandstones, heteroliths, calcareous sandstones	K-feldspars	kaolinite, chamosite, calcareous cementation	secondary	30–70	<(-0.15)	42, 44, 39, 37
S4	subarkosic and sublithic sandstones	K-feldspars, illite, muscovite	kaolinite, various cementation	secondary		>(–0.15)	103, 104, 100

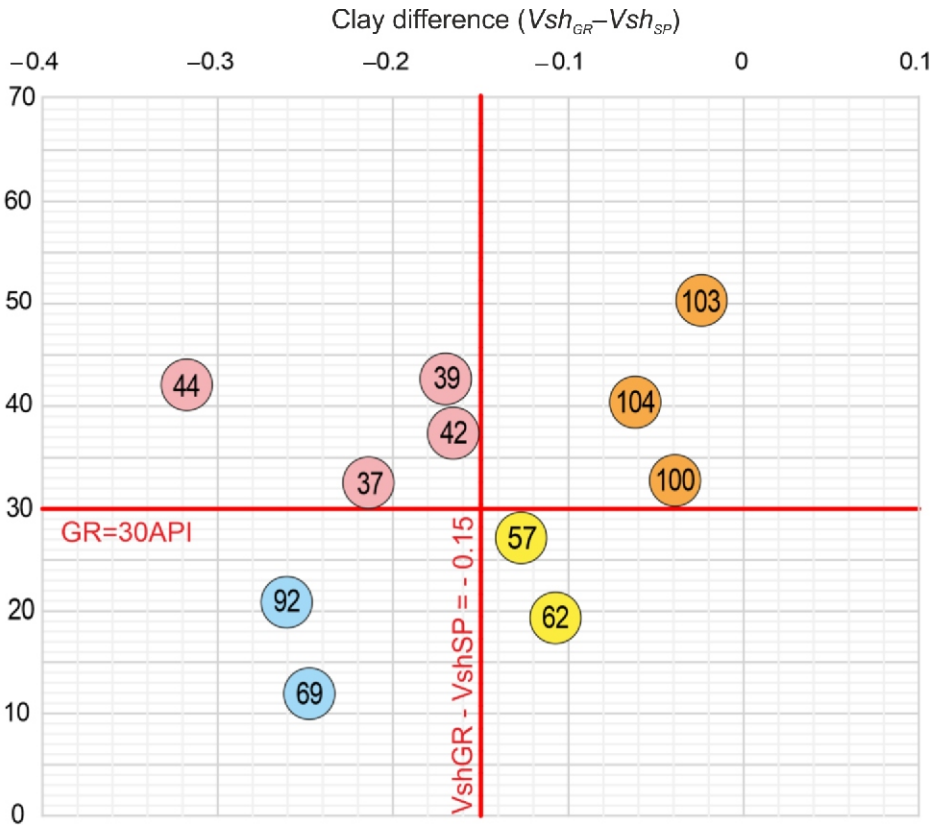

Fig. 6. Cross-plot of gamma ray and clay difference measurements with selected limit values of *GR* and clay difference defined based on available core samples

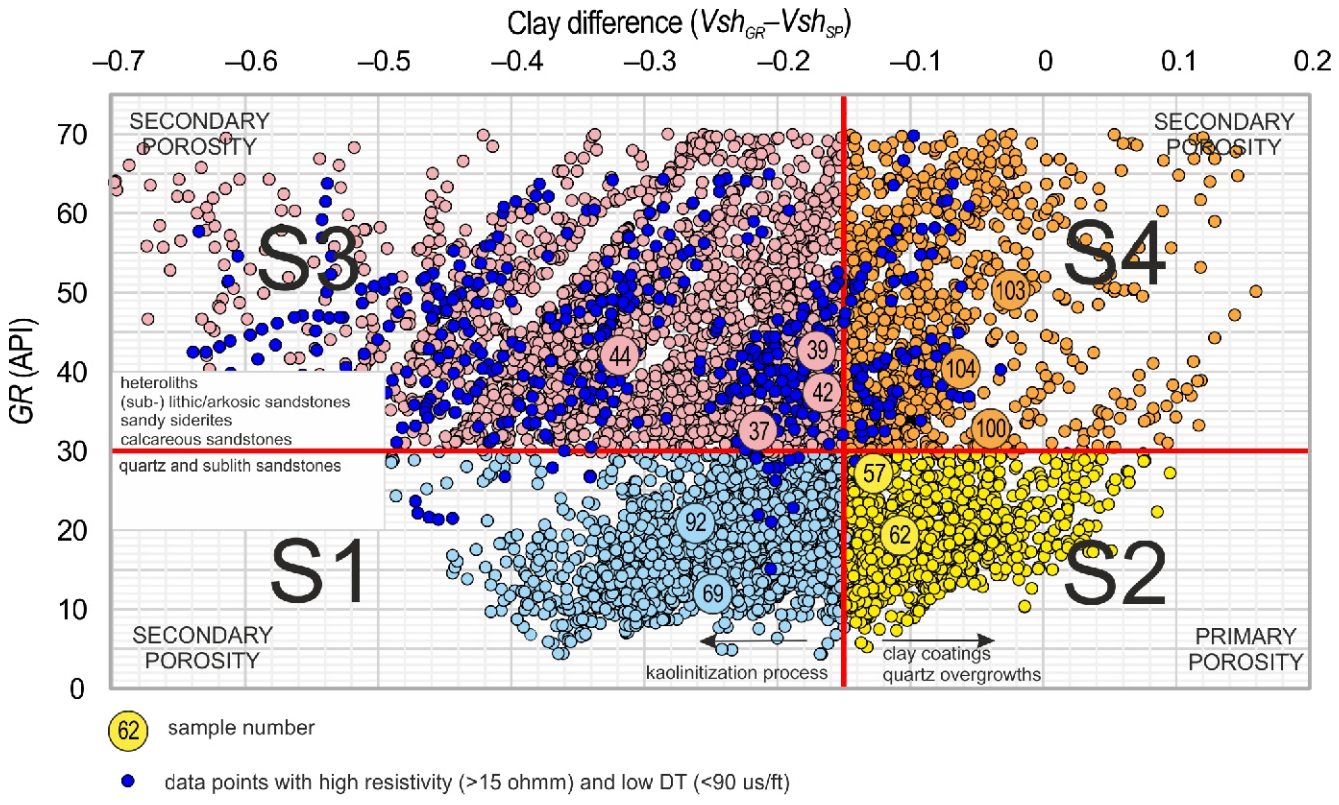

Fig. 7. Cross-plot of gamma ray and clay difference measurements with highlighted sandy petrofacies and their specific petrographic features

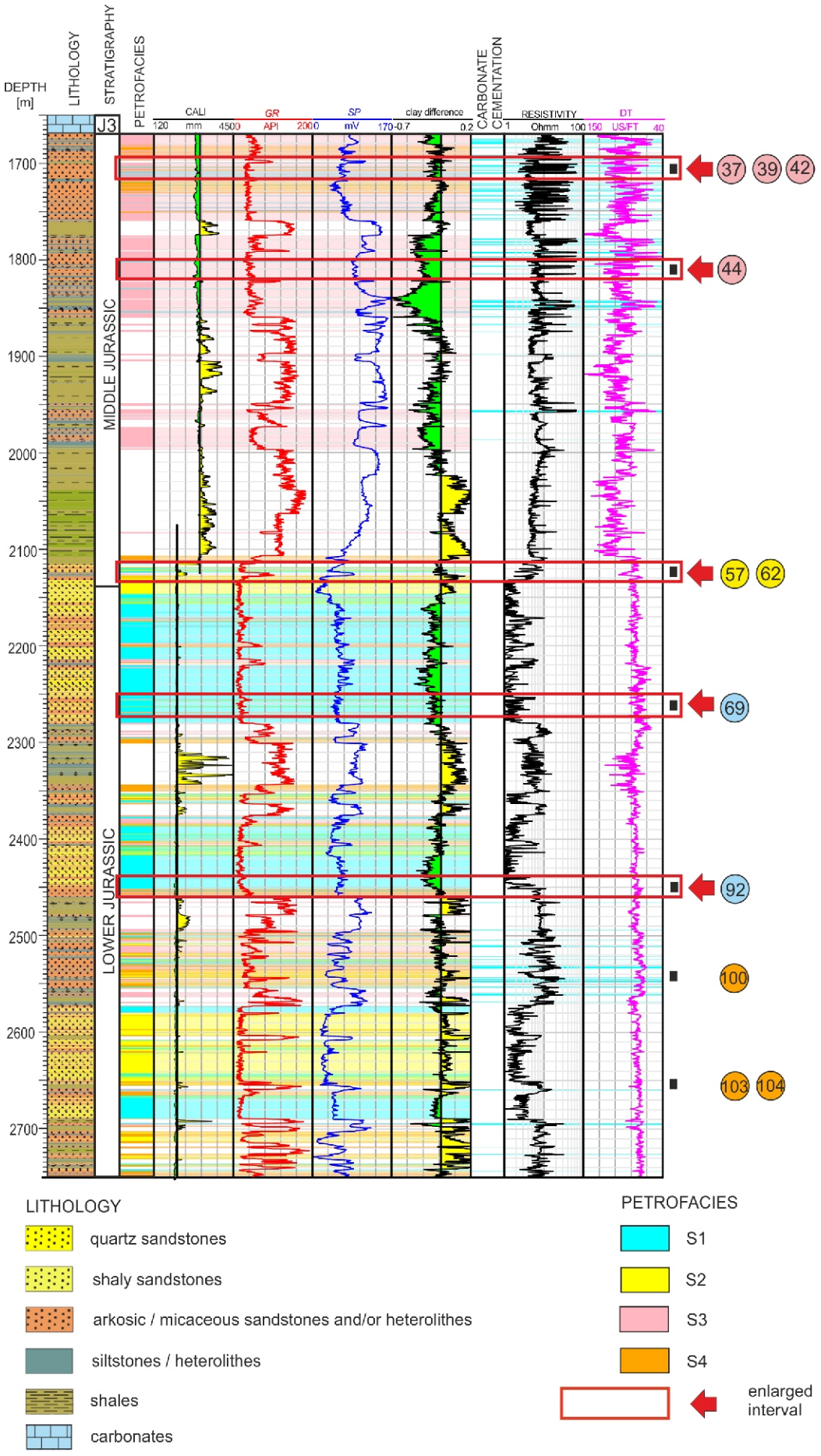

Fig. 8. Results of the petrofacies analysis with highlighted carbonate cemented intervals in Z-GN4 borehole

Stratigraphy log after Marek et al. (1992); lithology log made based on the borehole documentation, core and log interpretation (Karelus et al., 1992)

logs. Based on that, the value –0.15 was chosen to divide petrofacies S1 and S3 characterized by better petrophysical properties from S2 and S4. In addition, the intensely carbonate-cemented sandstone intervals were detected on the basis of their low sonic and high resistivity values. Finally, the data were integrated with archival petrophysical and XRD results (Karelus et al., 1992).

Complete petrofacies analysis (Fig. 8) was fundamental to characterizing the probable primary mineral composition and diagenetic features representing the range of reservoir parameters in these Jurassic sandstones.

DISCUSSION

In an era of global concern for our planet, it is our responsibility to mitigate the environmental impact of natural resources exploration. Moreover, the search for new deposits leads geologists to the most remote corners of the world, where access to modern data is often limited. For these reasons, special attention should be paid to the maximum use of available geological information to limit the drilling of new boreholes, which, apart from environmental benefits, may bring great savings to exploration companies.

Archival data analysis can be controversial because usually, it is impossible to support interpretations with modern geochemical measurements. This insufficient reliability makes them often neglected in advanced reservoir modeling processes. However, apart from basic geophysical measurements, very often archival borehole documentations contain much additional information that can be used to support more advanced interpretations. These are most often laboratory measurements of porosity and permeability, usually supplemented with bulk density and carbonate content. In addition, selective geochemical (XRD, SEM) and petrographic analyses of geological samples collected from boreholes have often been performed in the past. This information, especially geochemical, is often overlooked or considered unreliable in the context of modern analyses. However, study procedures often have not changed significantly, with the only complication being the unclear presentation of results.

Using archival geophysical and petrographic data from the borehole Z-GN4, an analysis of sandstone petrofacies was made, supplemented with laboratory data of porosity, permeability, density and the results of XRD geochemical analyses. Based on these results, conclusions were drawn about the primary mineral composition of sandstones, their secondary diagenetic transformations, and associated reservoir properties.

INFLUENCE OF NON-RADIOACTIVE CLAY MINERALS ON GAMMA RAY AND SPONTANEOUS POTENTIAL LOGS – S1 PETROFACIES

Cementation and grain-dissolution processes are common in the Jurassic clastic successions in the Z-GN4 core-section, with kaolinite a product of feldspar, lithic grains, and/or glauconite alteration (Churchman et al., 2012). This rock component does not emit such high natural radioactivity as do other clay minerals and its presence cannot be observed on the gamma ray log (Fig. 9), but is visible in XRD data from the section analysed (Fig. 13). The residual feldspar and glauconite fragments slightly increase the natural radioactivity of the sandstone. Kaolinite in the Z-GN4 sandstones is seen in petrographic thin section as a grain replacement or as a pseudomatrix filling pore space in quartz and/or sublithic, quartzitic arenites (Fig. 9). In some Jurassic formations, chlorite is also common. The presence of non-radioactive clay minerals is probably the main reason for the shale volume calculated from the *SP* log increase and causes the negative values in the clay difference curve in the kaolinite-rich sandstones. However, the porosity and permeability of the S1 petrofacies demonstrate the highest values among the petrofacies recognised to locally exceed 300 mD of permability and 25% of porosity (Figs. 11–13). Moreover, the bulk density of the samples analysed is generally low (1.9–2.3 g/cm^3) which is typical for porous sandstones. This is probably the result of secondary microporosity developed between kaolinite crystals (Ulmer-Scholle et al., 2014). Nevertheless, some of the S1 sandstones are characterized by moderate petrophysical properties, most likely caused by cementation and/or compaction in the clean quartz or quartzitic litharenites.

PRIMARY POROSITY PRESERVATION – S2 PETROFACIES

Some of the Lower and Middle Jurassic sandstones show good reservoir properties. Petrofacies S2 is characterized by low natural gamma radioactivity and positive values of clay difference. This is most likely caused by the low general shale content in the quartz and quartzitic sandstones and moderately high porosity (Figs. 9, 12 and 13). In some of the analysed samples of petrofacies S2, diagenetic processes such as a generation of quartz overgrowths (Fig. 10C) preserved the primary porosity from mechanical compaction. In others, however, the presence of primary clay coatings was the main reason why the primary pore space was prevented from generating secondary mineralization (Fig. 10A, B). These factors seem to be essential for preserving the primary porosity. However, they also reduce the connections between rock pores, which leads to a reduction in the permeability, which is consistent with this petrofacies being characterized by moderate permeabilities ranging <25 to 50 mD (Fig. 14).

CONDENSED, CLAYEY SANDY SIDERITES, CARBONACEOUS SANDSTONES AND HETEROLITHIC DEPOSITS – S3 PETROFACIES

The S3 petrofacies is characterized by the worst petrophysical parameters (Figs. 13 and 14), being mostly represented by condensed, clayey siderites, carbonaceous sandstones and heterolithic deposits. Petrofacies S3 generates higher natural gamma radioactivity, of from 30 to 70 API (Fig. 11). This is probably caused by the high content of radioactive clay minerals such as illite and/or glauconite. However, some of the condensed layers can exhibit higher uranium contents which can be the reason for the gamma ray increase (Vail et al., 1984; Loutit et al., 1988).

Besides primary composition, the diagenetic features define the value of clay difference. In the sandy siderites with clayey, microcrystalline siderite occupying the pore space (Fig. 11) clay difference shows negative values. Variable petrophysical parameters (Figs. 13 and 14) are caused by the secondary porosity which is the result of cement dissolution (Fig. 12B) or the bioturbation of heterolithic deposits (Fig. 12A). Petrofacies S3 mostly dominates the upper part of the Z-GN4 borehole, and includes siderite-rich layers and carbonaceous sandstones typical of the upper part of the Middle Jurassic succession.

CARBONACEOUS, SUBARKOSIC / SUBLITHIC SANDSTONES – S4 PETROFACIES

The mineral composition of petrofacies S4 is the most diverse. High gamma ray values are caused by radioactive minerals such as potassium feldspars, glauconite, muscovite, and/or illite, their presence being shown by XRD analysis

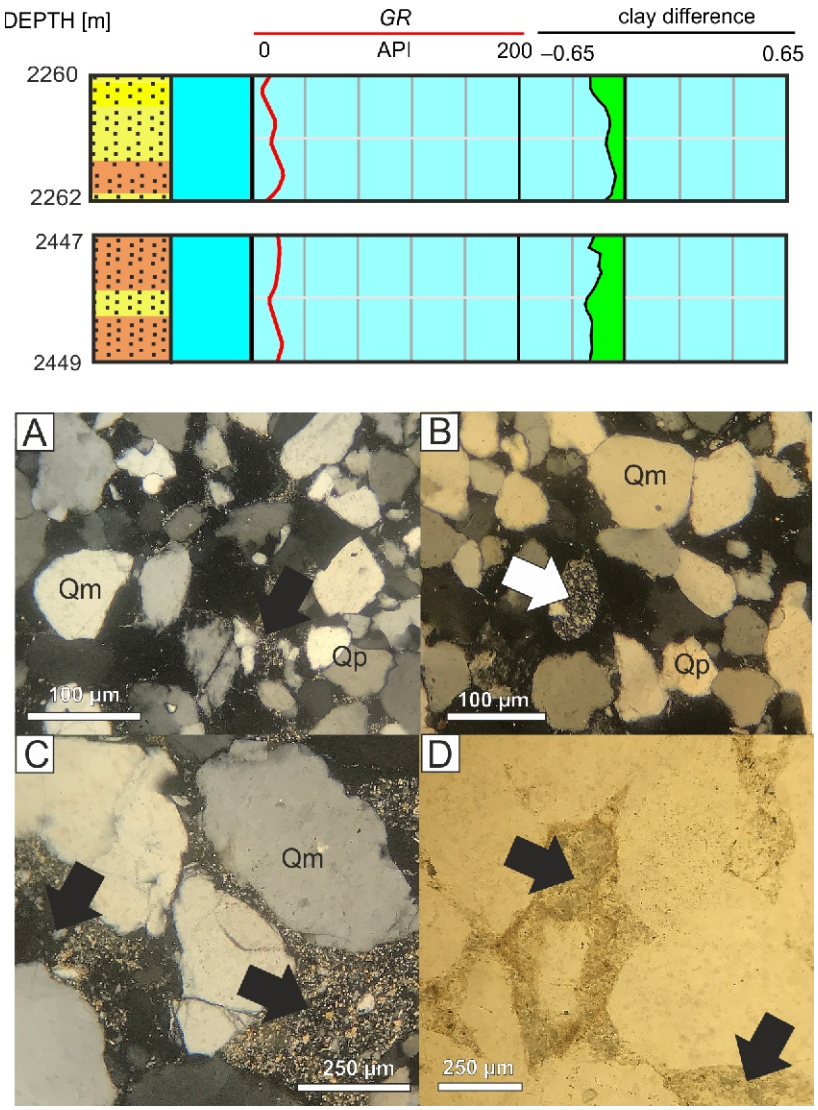

Fig. 9. Gamma ray and clay difference log response of petrofacies S1 compared with the primary mineral composition and diagenetic features visible in thin section microphotographs

A, B – sample 69, crossed polars, depth: 2260.45 m; **C** – sample 92, crossed polars, depth: 2447.45 m; **D** – sample 92, plane parallel light, depth: 2447.45 m; Qm – monocrystalline quartz, Qp – polycrystalline quartz, black arrow – kaolinite filling of the pore-space / clay coating, white arrow – kaolinite replacement of detrital grain

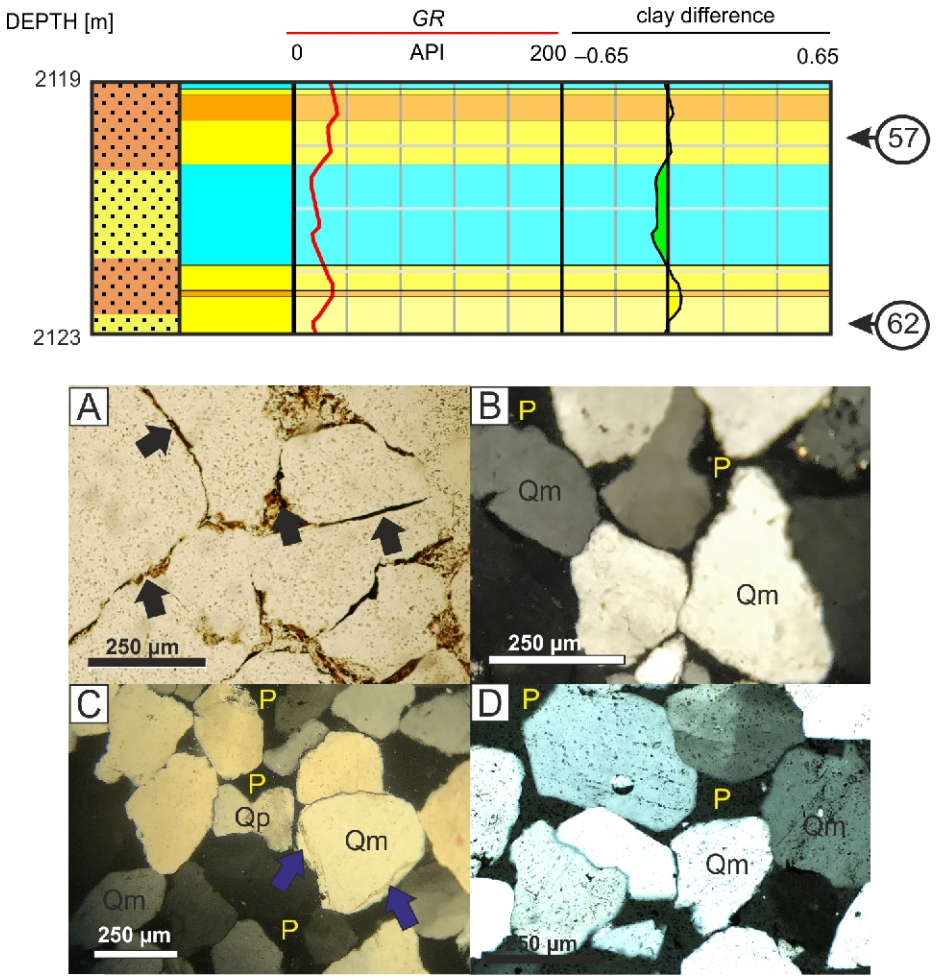

Fig. 10. Gamma ray and clay difference log response of petrofacies S2 compared with the primary mineral composition and diagenetic features visible in thin section microphotographs

A – primary clay coatings, plane parallel light, sample 57, depth: 2119.95 m; **B** – sample 57, crossed polars, depth: 2119.95 m; **C**, **D** – sample 62, crossed polars, depth: 2122.75 m; P – pore space, dark blue arrow – authigenic quartz overgrowths, black arrow – kaolinite filling of the pore-space / clay coating; other explanations as in Figure 9

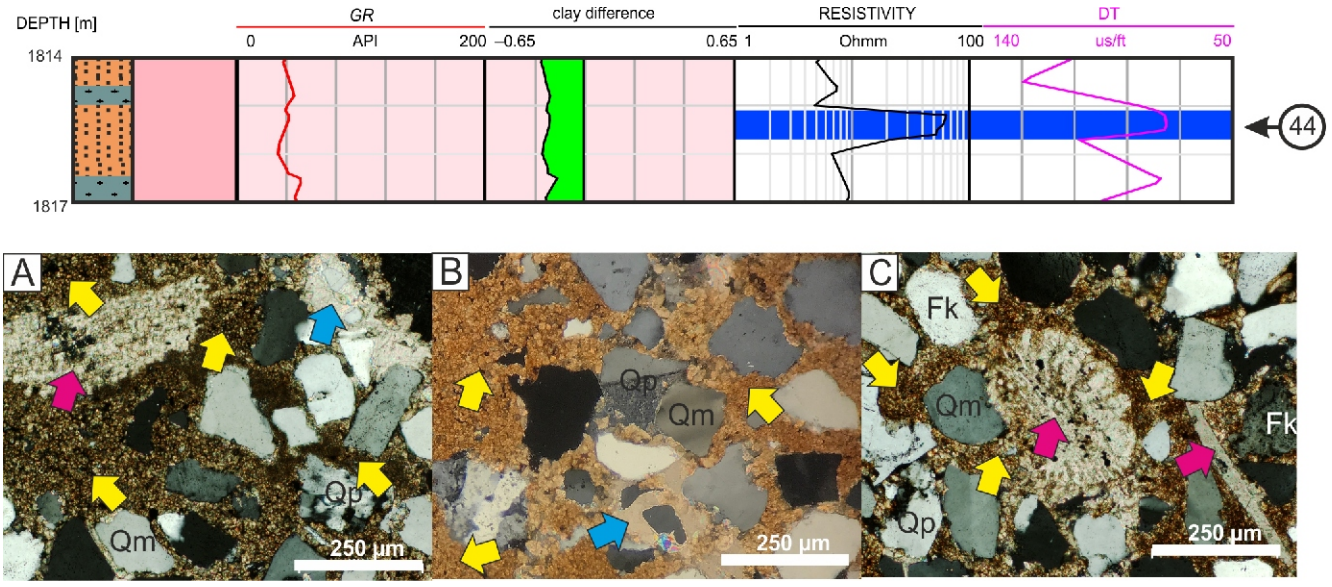

Fig. 11. Gamma ray, clay difference, deep resistivity and sonic log response of petrofacies S3 compared with the primary mineral composition and diagenetic features visible in thin section microphotographs

A – calcareous fossil surrounded by microcrystalline siderite, grain replacement; **B** – microcrystalline siderite, grain replacement; **C** – calcareous fossils surrounded by microcrystalline siderite, sample 44, crossed polars, depth: 1815.25 m: Fk – potassium feldspar, light blue arrow – calcareous cement, yellow arrow – microcrystalline siderite, dark pink arrow – calcareous echinoderm microfossils; other explanations as in Figure 9

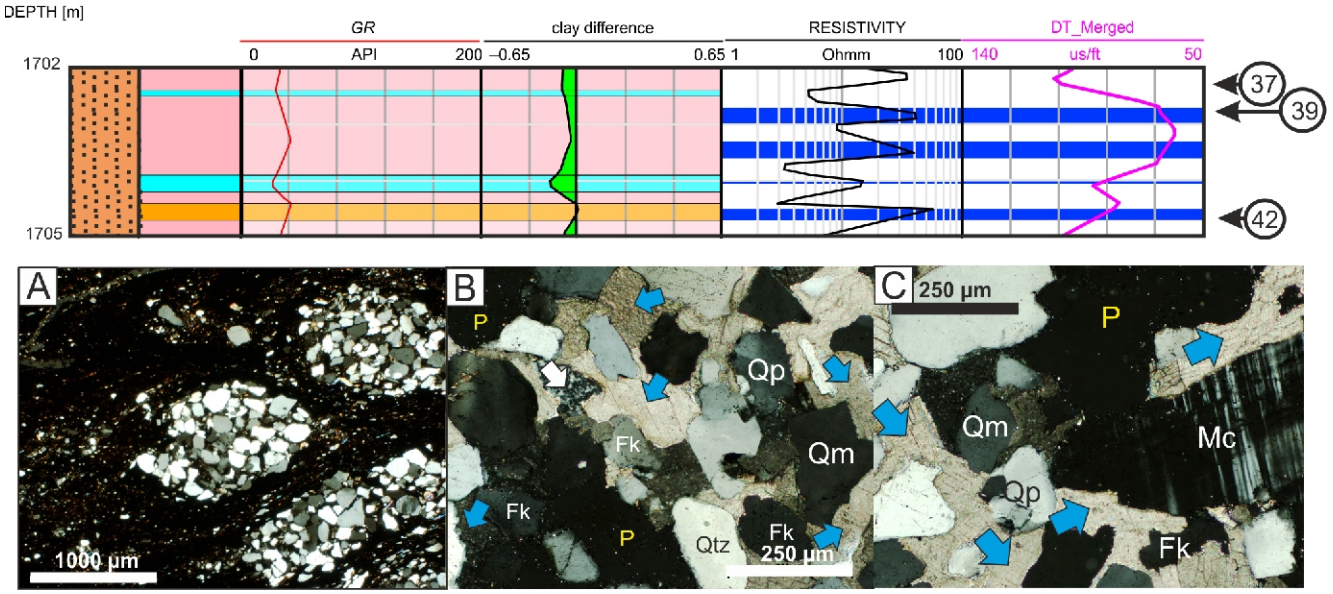

Fig. 12. Gamma ray, clay difference, deep resistivity, and sonic log response of petrofacies S3 and S4 compared with the primary mineral composition and diagenetic features visible in thin section microphotographs

A – bioturbation of heterolithic deposit, sample 37, crossed polars, depth: 1702.2 m; **B** – kaolinization and calcareous cementation in sandstone, sample 39, crossed polars, depth: 1703.25 m; **C** – calcareous cementation in sample 42, crossed polars, depth: 1704.65 m; Mc – microcline, light blue arrow – calcareous cement; other explanations as in Figure 11

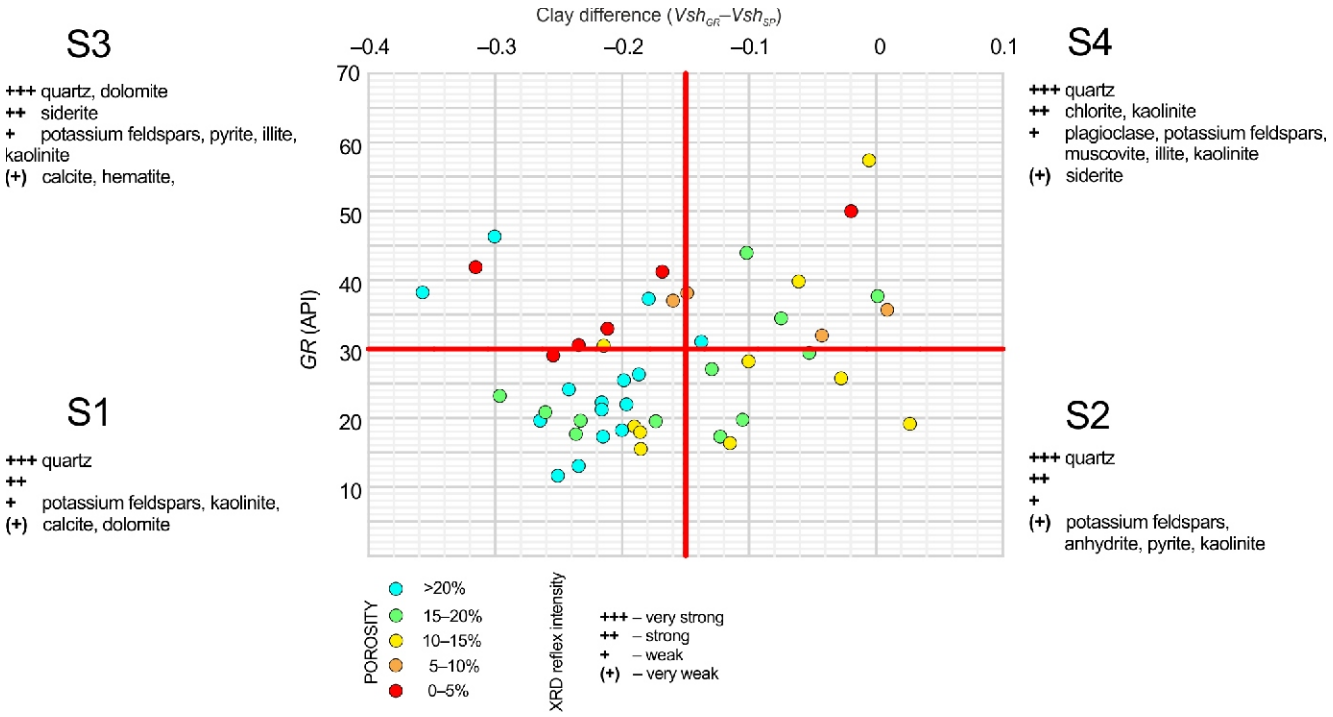

Fig. 13. Results of porosity measurements and XRD analysis of core samples from borehole documentation (Kopczyński et al., 1992; Waś et al., 1992) shown on the gamma ray and clay difference cross-plot

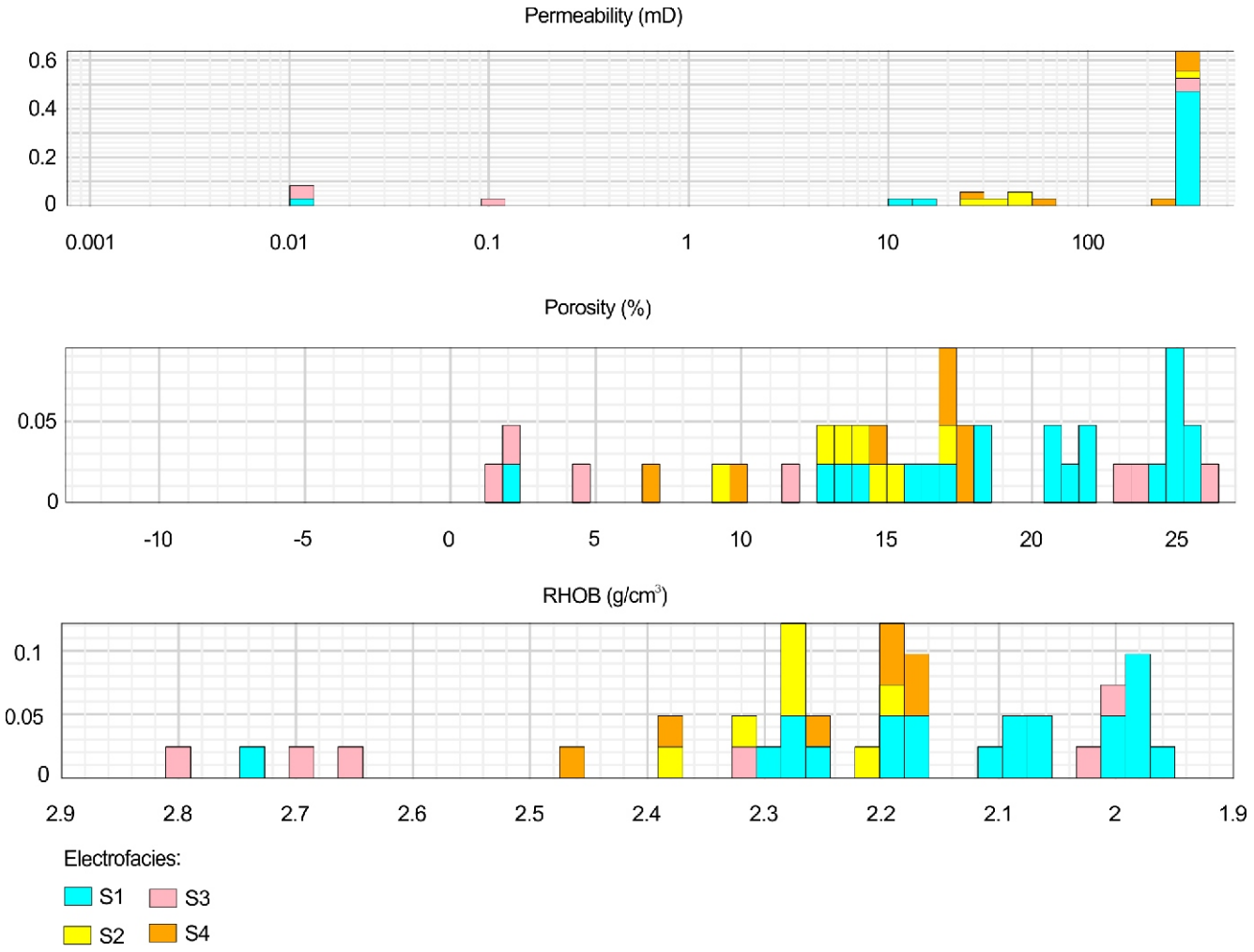

Fig. 14. Results of permeability, porosity and bulk density lab-measurements of core samples from borehole documentation (Kopczyński et al., 1992) shown on histograms

(Kopczyński et al., 1992; Fig. 13). However, clay difference values over –0.15 and variable petrophysical properties (Figs. 13 and 14) is most likely the reason of the high secondary porosity formed as a result of kaolinization or calcareous cement dissolution (Fig. 12C). Intercalations of petrofacies S4 are present throughout the profile.

RECOGNITION OF CARBONATE-CEMENTED INTERVALS IN THE Z-GN4 BOREHOLE USING RESISTIVITY AND ACOUSTIC LOGS

Carbonate cementation is mostly common in sandstones in the uppermost part of the profile (Fig. 8). It is dominant in petrofacies S3, less common in S4. It also occasionally occurs in petrofacies S1 (Fig. 7) as shown by XRD results (Karelus et al., 1992; Fig. 13). Siderite and dolomite cements occupying the pore space (Figs. 11 and 12B, C) are the reason for higher tortuosity of the remaining pores, which can lead to full impermeabilty to formation fluids. The influence of carbonaceous cementation in petrofacies S1 and S3 is visible in bulk density lab-measurements which can rise until 2.7–2.8 g/cm^3, values typical of carbonates (Fig. 14). Petrographic analysis of core samples confirmed the presence of intense carbonate cementation in layers of DT (<90 µs/ft) and higher (>15 ohmm) resistivity values depending on the remaining porosity of the layer (Fig. 13). This method additionally shows the increasing carbonate content towards the top of the clastic Middle Jurassic succession in the Z-GN4 borehole.

CONCLUSIONS

The integration of various archival well data can help to indicate sandy lithotypes with specific diagenetic and petrophysical features in un-cored intervals which can be useful in further reservoir characterization. The conclusions are as follows:

- The application of a clay difference log to the archival dataset for borehole Z-GN4 was the basis for distinguishing sandy rocks rich in less-radioactive clay minerals, especially kaolinite which is a product of mineral/lithic grain alteration and which cannot be observed by the most commonly used gamma ray clay volume calculation. The presence of diagenetic kaolinite is even more important because it can create secondary microporosity which enhances the sandstone reservoir parameters.
- Application of deep resistivity together with sonic measurements helped to distinguish carbonate-cemented intervals in the Z-GN4 borehole. This method seems to be helpful to demonstrate the increase of carbonate content in sandy rocks toward the top of the Middle Jurassic

succession in the Polish Basin. Moreover, the presence of the calcareous fossils in sample 44 supports the thesis of the biogenic origin of cement in the condensed layers. The carbonate skeleton fragments provide the main source of calcareous cement in shoreface sandstones, carbonate cementation being the result of diffusion (Bjørkum and Walderhaug, 1990; Maliszewska, 1998). Strongly carbonate-cemented intervals can be a perfect barrier for fluid flow and therefore can play the role of a secondary seal in the petroleum system.

– The petrofacies analysis example of borehole Z-GN4 was the basis to distinguish four different sandy petrofacies with different primary and diagenetic features consistent with the archival geochemical and petrophysical results.
– The application of petrofacies analysis can be helpful in detailed interpretation of archival geological and geophysical datasets when the core is no longer available but detailed correlation is necessary.

Acknowledgements. The author would like to express her sincere thanks to the Polish Oil and Gas Company for their assistance in providing the information, and for their technical input to this work. The author especially wishes to thank Dr M. Kozłowska, Prof. dr hab. A. Wysocka, Dr Y. Spychala, Dr A. Feldman-Olszewska and an anonymous reviewer whose suggestions and assistance significantly improved the quality of this paper.

REFERENCES

Adeoti, L., Ayolabi, E.A., James, P.L., 2009. An integrated approach to volume of shale analysis: Niger Delta example, Offrire Field. World Applied Sciences Journal, **7**: 448–452.

Bakke, N.E., 1996. Prediction of calcite cement distribution in shallow marine sandstone reservoirs using seismic data. Dissertation, Norwegian University of Science and Technology.

Bhattacharya, S., Doveton J.H., Carr, T.R., Guy, W.R., Gerlach, P.M., 2005. Integrated core-log petrofacies analysis in the construction of a reservoir geomodel: a case study of a mature Mississippian carbonate reservoir using limited data. AAPG Bulletin, **89**: 1257–1274.

Bjørkum, P.A., Walderhaug, O., 1990. Geometrical arrangement of calcite cementation within shallow marine sandstones. Earth-Science Reviews, **29**: 145–161.

Bolesta, F., Gałązka, A., 2014. Profilowanie gamma – przeliczanie jednostek (in Polish). Nafta-Gaz, **70**: 493–501.

Churchman, G.J., Lowe, D.J., 2012. Alteration, Formation, and Occurrence of Minerals in Soils. CRC press.

Cui, Y., Wang, G., Jones, S.J., Zhou, Z., Ran, Y., Lai, J., Deng, L., 2017. Prediction of diagenetic facies using well logs – a case study from the upper Triassic Yanchang Formation, Ordos Basin, China. Marine and Petroleum Geology, **81**: 50–65.

Dadlez, R., 1998. Devonian to Cretaceous epicontinental basins in Poland: relationship between their development and structure (in Polish with English summary). Prace Państwowego Instytutu Geologicznego, **165**: 17–30.

Dadlez, R., Marek, S., 1969. Structural style of the Zechstein–Mesozoic complex in some areas of the Polish Lowland. Geological Quarterly, **13**: 543–565.

Dadlez, R., Narkiewicz, M., Stephenson, R.A., Visser, M.T.M., Van Wees, J.D., 1995. Tectonic evolution of the Mid-Polish Trough: modelling implications and significance for central European geology. Tectonophysics, **252**: 179–195.

Dadlez, R., Jóźwiak, W., Młynarski, S., 1997. Subsidence and inversion in the western part of Polish basin – data from seismic velocities. Geological Quarterly, **41**: 197–208.

Dadlez, R., Marek, S., Pokorski, J., 1998. Paleogeographic atlas of epicontinental Permian and Mesozoic in Poland (1:2 500 000). Państwowy Instytut Geologiczny, Warszawa.

Dayczak-Calikowska, K., 1964. Atlas geologiczny Polski – Zagadnienia stratygraficzno-facjalne, z. 9 Jura, cz. II Jura środkowa (in Polish). Wyd. Geol., Warszawa.

Dayczak-Calikowska, K., 1967. Problems of Middle Jurassic stratigraphy in Poland. Biuletyn Instytutu Geologicznego, **203**: 59–83.

Dayczak-Calikowska, K., 1997. Middle Jurassic. Sedimentation, paleogeography and paleotectonics (in Polish with English summary). Prace Państwowego Instytutu Geologicznego, **153**: 269–282.

Dayczak-Calikowska, K., Moryc, W., 1988. Evolution of sedimentary basin and palaeotectonics of the Middle Jurassic in Poland (in Polish with English summary). Geological Quarterly, **32**: 117–136.

De Ros, L.F., Goldberg, K., 2007. Reservoir petrofacies: a tool for quality characterization and prediction. AAPG Search and Discovery, **50055**: 1–6.

Deczkowski, Z., 1997. Lower Jurassic. Sedimantation, paleogeography and paleotectonics (in Polish with English summary). Prace Państwowego Instytutu Geologicznego, **153**: 208–217.

Dembicz, K., Praszkier, T., 2003. Stratygrafia, mikrofacje i środowisko sedymentacji osadów keloweju z profilu Włodowice koło Zawiercia (in Polish). Tomy Jurajskie, **1**: 35–48.

Epov, M.I., Sukhorukova, K.V., Nechaev, O.V., Petrov, A.M., Rabinovich, M., Weston, H., Tyurin, E., Wang, L., Abubakar, A., Claverie, M., 2020. Comparison of the Russian and Western resistivity logs in typical Western Siberian reservoir environments: A numerical study. Petrophysics, **61**: 38–71.

Feldman-Olszewska, A., 1997a. Depositional architecture of the Polish epicontinental Middle Jurassic basin. Geological Quarterly, **41**: 491–508.

Feldman-Olszewska, A., 1997b. Depositional systems and cyclicity in the intracratonic Early Jurassic basin in Poland. Geological Quarterly, **41**: 475–490.

Feldman-Olszewska, A., 1998. Lower and Middle Jurassic. In: Palaeogeographical Atlas of the Epicontinental Permian and Mesozoic in Poland (eds. R. Dadlez, S. Marek and J. Pokorski). Państwowy Instytut Geologiczny, Warszawa.

Feldman-Olszewska, A., 2006. Sedimentary environments of the Middle Jurassic epicontinental deposits from the central part of the Polish Basin (Kuyavian Region). Volumina Jurassica, **4**: 86–86.

Furgał, G., 2003. Reinterpretacja archiwalnych danych geofizyki wiertniczej w otworach z obszaru syneklizy perybałtyckiej (in Polish). Przegląd Geologiczny, **51**: 793–794.

Gibbons, K., Hellem, T., Kjemperud, A., Nio, S.D., Vebenstad, K., 1993. Sequence architecture, facies development and carbonate-cemented horizons in the Troll Field reservoir, offshore Norway. Advances in Reservoir Geology: 1–31.

Girard, J.P., 1998. Carbonate cementation in the Middle Jurassic Oseberg Reservoir Sandstone, Oseberg Field, Norway: a case of deep burial–high temperature poikilotopic calcite. In: Carbonate Cementation in Sandstones (eds. R. Worden and S. Morad): 285–307.

Giżejewska, M., Wieczorek, J., 1976. Remarks on the Callovian and Lower Oxfordian of the Zalas Area (Cracow Upland, Southern Poland). Bulletin de l'Academie Polonaise des Sciences, Série des Sciences de la Terre, **24**: 167–175.

Głazek, J., Kutek, J., 1976. Powaryscyjski rozwój geotektoniczny obszaru świętokrzyskiego (in Polish). Przewodnik XLVIII Zjazdu Polskiego Towarzystwa Geologicznego, Starachowice: 14–51.

Gutowski, J., Krzywiec, P., Walaszczyk, I., Pożaryski, W., 2003. Od ekstensji do inwersji – zapis aktywności północno-wschodniej brzeżnej strefy uskokowej świętokrzyskiego segmentu bruzdy śródpolskiej w osadach jury górnej i kredy na podstawie interpretacji danych sejsmiki refleksyjnej (in Polish). Volumina Jurassica, **1**: 124–125.

Harrison, B. (ed.), 1995. Russian-Style Formation Evaluation. Geological Society of London.

Ingersoll, R.V., 1990. Actualistic sandstone petrofacies: discriminating modern and ancient source rocks. Geology, **18**: 733–736.

Jahan, C.S., Islam, M.A., Mazumder, Q.H., Asaduzzaman, M., Islam, M.M., Islam, M.O., Sultana, A., 2007. Evaluation of depositional environment and aquifer condition in Barind area, Bangladesh using gamma ray well log data. Journal Geological Society of India, **70**: 1070.

Jarzyna, J., Bała, M., Zorski, T., 1999. Metody geofizyki otworowej: pomiary i interpretacja (in Polish). AGH Uczelniane Wydawnictwa Naukowo-Dydaktyczne.

Karelus, U., Kaczyński, J., Modzelewski, R., Nocoń, W., 1992. Dokumentacja Wynikowa Odwiertu Poszukiwawczego Z-GN4 (in Polish). NAG (nr 133135), Warszawa.

Karnkowski, P.H., 1999. Origin and evolution of the Polish Rotliegend Basin. Polish Geological Institute Special Papers, **3**: 1–93.

Kopczyński, R., Boguszewska, K., Derewecka, J., Rochewicz, A., 1992 Analizy fizyczne rdzeni (in Polish). In: Dokumentacja Wynikowa Odwiertu Poszukiwawczego Z-GN4. NAG (nr 133135), Warszawa.

Kopik, J., 1998. Lower and Middle Jurassic of the north-eastern margin of the Upper Silesian Coal Basin (in Polish with English summary). Biuletyn Państwowego Instytutu Geologicznego, **378**: 67–120.

Kosakowski, P., Wójcik-Tabol, P., Kowalski, A., Zacharski, J., 2015. Jurassic petroleum system in the Polish Lowlands (Central Poland) – organic geochemical and numerical modelling approach. 77th EAGE Conference and Exhibition 2015. Earth Science for Energy and. Environment: 2181–2185.

Kotański, Z. (ed.), 1997. Geological Atlas of Poland – Geological Maps of Horizontal Cutting 1:750 000. Wydawnictwa Kartograficzne Polskiej Agencji Ekologicznej.

Kozłowska, K., Kuberska, M., 2014. Diagenesis and porosity of the Lower Jurassic sandstones in the Polish Lowlands (in Polish with English summary). Biuletyn Państwowego instytutu Geologicznego, **458**: 39–60.

Krzywiec, P., Kramarska, R., Zientara, P., 2003. Strike-slip tectonics within the SW Baltic Sea and its relationship to the Mid-Polish Trough inversion – evidence from high-resolution seismic data. Tectonophysics, **373**: 93–105.

Krzywiec, P., 2006. Structural inversion of the Pomeranian and Kuiavian segments of the Mid-Polish Trough – lateral variations in timing and structural style. Geological Quarterly, **50**: 151–168.

Lai, J., Wang, G., Wang, S., Cao, J., Li, M., Pang, X., Zhou, Z., Fan, X., Dai, Q., Yang, L., He, Z., Qin, Z., 2018. Review of diagenetic facies in tight sandstones: Diagenesis, diagenetic minerals, and prediction via well logs. Earth-Science Reviews, **185**: 234–258.

Lai, J., Fan, X., Liu, B., Pang, X., Zhu, S., Xie, W., Wang, G., 2020. Qualitative and quantitative prediction of diagenetic facies via well logs. Marine and Petroleum Geology, **120**:104486.

Leonowicz, P., 2005. The Ciechocinek Formation (Lower Jurassic) of SW Poland: Petrology of green clastic rocks. Geological Quarterly, **49**: 317–330.

Lewandowski, M., Krobicki, M., Matyja, B.A., Wierzbowski, A., 2005. Palaeogeographic evolution of the Pieniny Klippen Basin using stratigraphic and palaeomagnetic data from the Veliky Kamenets section (Carpathians, Ukraine). Palaeogeography, Palaeoclimatology, Palaecology, **216**: 53–72.

Loutit, T.S., Hardenbol, J., Vail, P.R., Baum, G.R., 1988. Condensed sections: the key to age-dating and correlation of continental margin sequences. SEPM Special Publication, **42**: 183–213.

Maliszewska, A., 1998. New petrological data on carbonate mineralogy in the Middle Jurassic siliciclastic deposits of the Kujawy region (Polish Lowlands). Geological Quarterly, **42**: 401–420.

Maliszewska, A., 1999. Middle Jurassic (in Polish with English summary). Prace Państwowego Instytutu Geologicznego, **167**: 1–154.

Marek, S., Pajchlowa, M. (eds.), 1997. Epicontinental Permian and Mesozoic in Poland (in Polish with English summary). Prace Panstwowego Instytutu Geologicznego, **153**.

Marek, S., Nocoń, W., Płachta, M., 1992. Profil odwietru faktyczny. In: Dokumentacja Wynikowa Odwiertu Poszukiwawczego Z-GN4 (in Polish). NAG (nr 133135), Warszawa.

Matyja, B.A., 1977. The Oxfordian in the south-western margin of the Holy Cross Mts. Acta Geologica Polonica, **27**: 41–64.

Matyja, B.A., 2015. Jurajska ewolucja północnego obrzeża Tetys (in Polish). Przewodnik LXXXIV Zjazdu Naukowego PTG: 9–11.09.2015, Chęciny: 28–40.

Matyja, B.A., Wierzbowski, A., 2006. The oceanic „Metis Geotectonic Event" (Callovian/Oxfordian) and its implications for the Peri-Tethyan area of Poland. Volumina Jurassica, **4**: 60–61.

Michalski, A., 1885. Formacja jurajska w Polsce (in Polish). Pamiętnik Fizjograficzny, **5**: 8–29.

Narkiewicz, M., Dadlez, R., 2008. Geological regional subdivision of Poland: general guidelines and proposed schemes of sub-Cenozoic and sub-Permian units (in Polish with English summary). Przegląd Geologiczny, **56**: 391–397.

Pettijohn, F.J., Potter, P.E., Siever, R., 1974. Sand and Sandstone. Springer, New York.

Pieńkowski, G., 2004. The epicontinental Lower Jurassic of Poland. Polish Geological Institute Special Papers, **12**.

Premik, J., 1933. Budowa i dzieje geologiczne okolic Częstochowy (in Polish). Drukarnia Wł. Łazarskiego.

Rider, M., 2002. The Geological Interpretation of Well Logs. Rider-French Consult. Ltd.

Serra, O., 1986. Fundamentals of Well Log Interpretation. Interpretation of Logging Data, **2**, Elsevier, Amsterdam.

Siemiątkowska-Giżejewska, M., 1974. Stratigraphy and paleontology of the Callovian in the southern and western margins of the Holy Cross Mts. Acta Geologica Polonica, **24**: 365–406.

Stephenson, R.A., Narkiewicz, M., Dadlez, R., Van Wees, J.D., Andriessen, P., 2003. Tectonic subsidence modelling of the Polish Basin in the light of new data on crustal structure and magnitude of inversion. Sedimentary Geology, **156**: 59–70.

Szabó, N.P., 2011. Shale volume estimation based on the factor analysis of well-logging data. Acta Geophysica, **59**: 935.

Szewczyk, J., 2000. Statistic-stratigraphic standarization of gamma ray measurements (in Polish with English summary). Biuletyn Państwowego Instytutu Geologicznego, **392**: 121–152.

Teofilak, A., 1960. Petrografia liasu I doggeru w wierceniu Gorzów Wielkopolski IG-1 (in Polish). NAG (nr 54429), Warszawa .

Teofilak, A., 1961. Petrografia liasu I doggeru w otworach Gołdap i Bartoszyce (in Polish). Profile głębokich otworów wiertniczych Instytutu Geologicznego, **14**: 283–291.

Teofilak, A., 1962. Jura dolna – Charakterystyka petrograficzna głównych typów skał; Dogger – Charakterystyka petrograficzna głównych typów skał (in Polish). In: Budowa geologiczna Niżu Polski (ed. W. Pożaryski): 203–206. Wydawnictwa Geologiczne, Warszawa.

Teofilak-Maliszewska, A., 1968. Mineralization of Dogger deposits in the borehole Głogowiec (in Polish with English summary). Geological Quarterly, **12**: 105–116.

Ulmer-Scholle, D.S., Scholle, P.A., Schieber, J., Raine, R.J., 2014. A color guide to the petrography of sandstones, siltstones, shales and associated rocks. AAPG Memoir, **109**.

Waś, K., Kopczyński, R., Rochewicz, A., 1992. Analizy rentgenowskie rdzeni (in Polish). In: Dokumentacja Wynikowa Odwiertu Poszukiwawczego Z-GN4. NAG (nr 133135), Warszawa

Willis, J.J., McIntosh Jr, D.S., Zwennes, J.W., Ferguson, G.J., 2017. Quick-look technique for quantifying shale distribution types using total porosity versus shale volume crossplots. Gulf Coast Association of Geological Societies Transactions, **67**: 539–549.

Wiltgen, N.A., 1994. The Essential Of Basic Russian Well Logs And Analysis Techniques. SPWLA 35th Annual Logging Symposium. Society of Petrophysicists and Well-Log Analysts, Tulsa, Oklahoma, June 1994.

Wróblewska, S., Kozłowska, M., 2019. Influence of primary composition and diagenetic mineralization on natural gamma ray and density logs of Carboniferous sandstones of the Dęblin Formation. Geological Quarterly, **63**: 741–756.

Vail, P.R., Hardenbol, J., Todd, R.G., 1984. Jurassic unconformities, Chronostratigraphy and sea-level changes from seismic stratigraphy and biostratigraphy. AAPG Memoir, **36**: 129–144.

Ziegler, P.A., 1990. Geological Atlas of Western and Central Europe, 2nd Ed. Shell Internationale Petroleum Maatschappij B. V. and The Geological Society Publishing House, Bath.

Znosko, J., 1957. Upward movements of Kłodawa salt diapir and its influence on genesis of sideritic coquinaes (in Polish with English summary). Geological Quarterly, **1**: 90–104.

Znosko, J., 1968. Transgressive oscilations of the Dogger sea between Gorzów Wielkopolski and Zakrzewo (in Polish with English summary). Geological Quarterly, **12**: 308–315.

Żelaźniewicz, A., Aleksandrowski, P., Buła, Z., Karnkowski, P.H., Konon, A., Oszczypko, N., Ślączka, A., Żaba, J., Żytko, K., 2011. Polska bez pokrywy kenozoicznej (in Polish). In: Regionalizacja tektoniczna Polski (ed. A. Żelaźniewicz): 25–28. Komitet Nauk Geologicznych PAN.